JOURNAL OF SOLID STATE CHEMISTRY **121,** 400–407 (1996)
ARTICLE NO. 0054

Metastable Nickel Sulfides with Composition Close to Ni_7S_6—Stability and Structural Properties

Helene Seim, Helmer Fjellvåg, Fredrik Grønvold, and Svein Stølen

Department of Chemistry, University of Oslo, Postbox 1033, N-0315 Oslo, Norway

Received August 8, 1995; in revised form October 23, 1995; accepted October 25, 1995

Four well-defined metastable phases with composition close to Ni_7S_6 are described. These phases are structurally closely related to the high-temperature phase $Ni_{7\pm x}S_6$, which is formed eutectoidally from Ni_9S_8 and Ni_3S_2 at ~675 K. The relative stability and a preliminary structural description of the metastable phases have been obtained from X-ray diffraction, transmission electron microscopy, calorimetry, and thermal analysis. Conditions for preparation of the different metastable phases are provided. On rapid quenching of $Ni_{7\pm x}S_6$ in ice + water + NaCl, an as-quenched state is obtained. This state is rather unstable and transforms on storing at room temperature to the metastable phase denoted α^{iv} and subsequently to α^{iii}. The actual phase sequence observed during heating of these modifications depends strongly on the thermal history of the sample and especially on the heating rate used in the experiments. Either of the two quasi-reversible phase sequences

$$\alpha^{iv} \Leftrightarrow \alpha^{ii} \Leftrightarrow \alpha^{i} \Leftrightarrow Ni_{7\pm x}S_6$$

or

$$\alpha^{iii} \Leftrightarrow \alpha^{i} \Leftrightarrow Ni_{7\pm x}S_6$$

is observed, where α^{i}, α^{ii}, α^{iii}, and α^{iv} denote the four well-defined metastable phases. The as-quenched samples appear rather similar to α^{i}. Furthermore, an exothermal phase transformation is observed for α^{iii}. It has not, however, been possible to relate this transformation to structural changes.

INTRODUCTION

The nickel sulfides and the phase relations in the Ni–S system have been the subject of numerous studies. For the interval between 45 and 48 mol% sulfur, a rather confusing situation with contradictory reports (1–8) has only partly been clarified, first through a single crystal diffraction study by Fleet on α-Ni_7S_6 (7), later by recognition of isostructurality between Ni_9S_8 (also termed β-Ni_7S_6) and the mineral godlevskite (8–11), and recently by the identification of several metastable phases (12–14). The complex situation in this part of the phase diagram was indicated already in the electron diffraction study by Putnis (15), who observed superstructure reflections for rapidly cooled samples of α-Ni_7S_6.

We have recently published heat-capacity results for the stable phases Ni_3S_2 (16), NiS (17), and Ni_7S_6 and Ni_9S_8 (13). These studies confirm that α-Ni_7S_6 (7) and Ni_9S_8 (11) (hereafter designated $Ni_{7\pm x}S_6$ and Ni_9S_8) are the only stable phases in the composition range from 45 to 48 mol% S. Whereas Ni_9S_8 is stoichiometric and stable below 709 ± 2 K, the nonstoichiometric $Ni_{7\pm x}S_6$ phase forms eutectoidally from Ni_9S_8 and Ni_3S_2 at ~675 K (13). The equilibrium phase diagram for the composition region 44–48 at.% S is shown in Fig. 1.

During the earlier studies of Ni_3S_2 (18) and of $Ni_{7\pm x}S_6$ and Ni_9S_8 (12–14), it became evident that rapid cooling of samples with composition within the stability region of the $Ni_{7\pm x}S_6$ phase leads to the occurrence of additional phases in this composition range. It was later shown that these additional phases disproportionate into two-phase mixtures of Ni_3S_2 and Ni_9S_8 on annealing not too far below the eutectoidal temperature; hence, metastability was suggested (13).

The present study concerns the stability and structural properties of metastable nickel sulfides with composition close to Ni_7S_6. Due to phase metastability, it is pertinent to describe the observed thermal behavior according to the heating rate adopted in the actual experiment. Thus, a distinction will be made between rapid heating (on the order of 1–10 $K \cdot min^{-1}$) and slow (on the order of days to weeks). In the present case, thermal analysis (DSC) and high-temperature X-ray diffraction (PXD), and adiabatic calorimetry and long-term annealing represent techniques used for studying the thermal evolution in the rapid and slow time regimes, respectively. The adopted Guinier–Simon X-ray diffraction technique provides continuous recording of the diffraction photographs as a function of temperature and/or time on the same film, thus enabling comparison of the different metastable phases and determination of the reversibility of the transitions. The results

0022-4596/96 $18.00

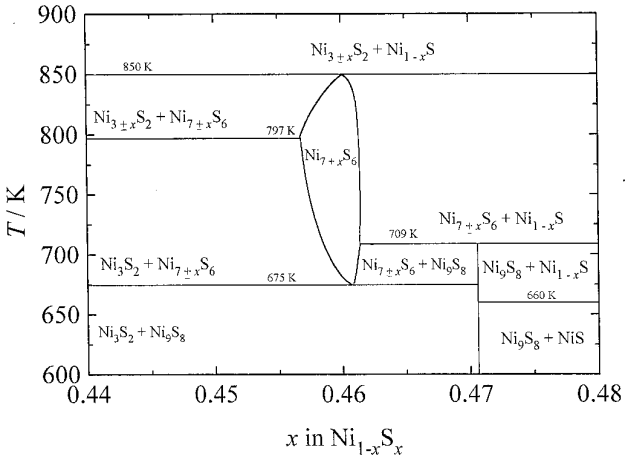

FIG. 1. Phase diagram for the Ni–S condensed system for $x_S = 0.44$ to 0.48.

are combined to give a description of the relative stability and, hence, provide conditions for the preparation of the different metastable phases. In order to establish an approximate relationship between the different modifications, a preliminary schematic description of three of the four metastable and structurally complex phases is included.

EXPERIMENTAL

Small-scale samples (0.5 to 1 g) were synthesized from the elements (Ni, 99.99%, Johnson Matthey Laboratories, turnings from rods, and S, 99.999%, Koch-Light Laboratories, small crystals) as starting materials. Some 30 samples with compositions between 44.8 and 47.8 mol% S were prepared. The samples were heated in sealed evacuated vitreous silica ampoules. After a first heat treatment at 823 K the samples were crushed at room temperature and subjected to two or three more annealing cycles until homogeneity was obtained. The homogeneous samples were thereafter divided into smaller portions, which in turn were heat treated at different temperatures (in 50 K intervals from 373 to 833 K). Two types of cooling procedures were adopted in the final heat treatment; quenching into an ice/water mixture and slow cooling within the furnace.

The large-scale sample (65 g), for the calorimetric measurements, was obtained by annealing the sample used in Ref. (13) at 750 K for 5 days. It was then quenched in a water–brine mixture, and annealed at 353 K for 3 months prior to the measurements.

All samples were characterized by powder X-ray diffraction (PXD) at room temperature, using Guinier–Hägg cameras (Cr$K\alpha_1$ or Cu$K\alpha_1$ radiation, Si as internal standard, $a = 543.1065$ pm (19)). $Ag_6Ge_{10}P_2$, with $a = 1031.25$ pm (20) was used as an internal standard for the metastable samples, since it gave several reflections at low scattering angles. High-temperature PXD photographs were taken at temperatures from 300 to 1200 K, with a Guinier–Simon camera (Enraf–Nonius FR 533; Cu$K\alpha_1$ radiation). The samples were measured in evacuated and sealed vitreous silica capillaries, and the temperature increase or decrease ($8–33\ K \cdot h^{-1}$) was synchronized with the translatory movement of the film cassette. The temperature readings were calibrated by measurements of the thermal expansivity of Ag (21). The films were evaluated visually by use of a film comparator. Unit-cell dimensions were obtained by least-squares refinement using the CELLKANT program (22). Theoretical powder diffractograms were calculated by means of the LAZY-PULVERIX program (23).

Differential scanning calorimetry (DSC) was carried out between 300 and 873 K using a Mettler TA3000 system. Heating and cooling rates were $10\ K \cdot min^{-1}$; onset temperatures for the thermal effects are given.

The high-temperature adiabatic calorimeter and measuring technique have been described earlier (24, 25). The 65-g Ni_7S_6 sample was enclosed in an evacuated vitreous silica tube of about 50 cm^3 volume which fits tightly into the silver calorimeter. The Pt-resistance thermometer was calibrated locally at the ice, steam, Sn, Zn, and Sb points. The temperatures were judged to correspond to IPTS-68 to within 0.05 K below 900 K and the heat capacity of the empty calorimeter was determined in a separate series of experiments. Corrections were applied for the differences in mass of the vitreous silica containers. In the present work, the calorimeter was used as an instrument for thermal analysis of slow phase transformations. Such transformations give rise to small, noninstrumental, positive or negative contributions to the temperature drift rate in the equilibration periods. The detection limit is, hence, determined by the temperature stability of the instrument (26).

RESULTS

(*i*) *Occurrence of the Metastable Phases*

It proved impossible to quench the high-temperature $Ni_{7\pm x}S_6$ phase and to retain the disordered orthorhombic structure (12, 13) under the experimental conditions used here. The powder X-ray diffraction results show that the quenching changes the phase into one or more metastable phases (see below) closely related to $Ni_{7\pm x}S_6$ in structure. It was realized that the tabulated powder X-ray diffraction pattern for $Ni_{7\pm x}S_6$ does not refer entirely to the high-temperature phase, designated α-Ni_7S_6 in the literature (7), but includes reflections from metastable species. This observation explains why several lines nonindexable in terms of the $Ni_{7\pm x}S_6$ unit cell have frequently been reported for samples in this composition range.

The as-quenched metastable product, as seen by PXD, changes nature on storing at room temperature for some

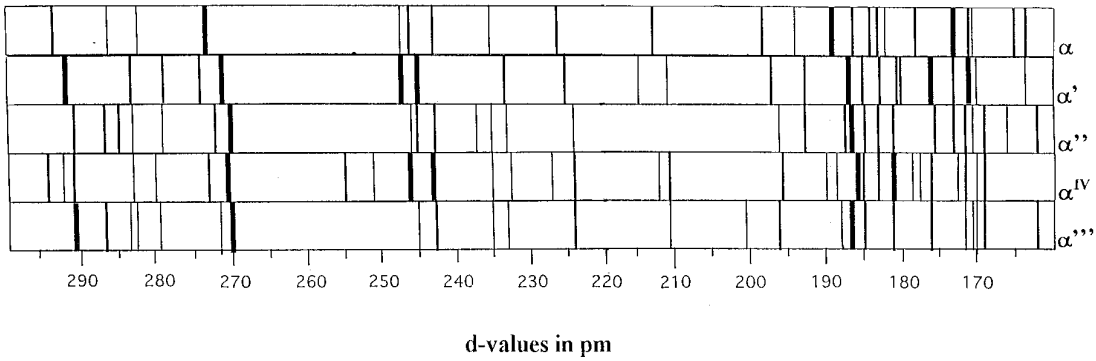

FIG. 2. Schematic drawing of the observed diffraction patterns for the different stable and metastable modifications of $Ni_{7\pm x}S_6$.

weeks into another metastable phase. Even though the as-quenched product is found to depend on the cooling rate to some extent, the resulting metastable phase is always the same. Its structure is kinetically very stable and the phase remains metastable at ambient temperature for prolonged periods of time. Annealing at higher temperatures, e.g., at 470 K up to some weeks, does not give the expected equilibrium mixture of Ni_9S_8 and Ni_3S_2. Trace amounts of Ni_3S_2 were, however, finally observed after 2 months annealing. When the annealing is performed at temperatures above 550 K the conversion of the metastable phase(s) into the stable two-phase mixture rapidly occurs.

Metastable phases are observed also on quenching samples with composition outside the $Ni_{7\pm x}S_6$ homogeneity region. Thus, when slightly more sulfur-rich samples are quenched from temperatures above the peritectoidal decomposition of Ni_9S_8 into $Ni_{1-x}S$ and $Ni_{7\pm x}S_6$, two-phase mixtures of $Ni_{1-x}S$ and metastable $Ni_{7\pm x}S_6$ phases are obtained. In such cases, achievement of thermodynamic equilibrium required relatively high annealing temperatures and/or long annealing times.

(*ii*) *Phase Changes of $Ni_{7\pm x}S_6$ on Annealing and Slow Heating*

X-ray photographs of Ni_7S_6 taken just after quenching show sharp Bragg reflections. During long-term storage at ambient temperature or by annealing at slightly elevated temperatures, e.g., 320 K, the as-quenched metastable samples transform into a single-phase metastable modification which is denoted α^{iv}-$Ni_{7\pm x}S_6$ (for practical reasons termed α^{iv}). Significant structural changes occur and several reflections become rather diffuse. The characteristic powder X-ray diffraction patterns are shown schematically in Fig. 2. Annealing of the as-quenched sample at a somewhat higher temperature, e.g., 350 K, gives the phase denoted α^{iii}-$Ni_{7\pm x}S_6$ (termed α^{iii}) (see Fig. 2 for the diffraction pattern), whereas annealing of α^{iv} at temperatures up to 485 K produces α^{ii}-$Ni_{7\pm x}S_6$ (termed α^{ii}), which subsequently disproportionates to the stable two-phase mixture of Ni_9S_8 and Ni_3S_2 at ~560 K. It should be noted that α^{iv} transforms directly to α^{ii} if heated so fast that α^{iii} is not formed. α^{iii} does not transform into α^{ii}, but directly to the stable two-phase mixture of Ni_9S_8 and Ni_3S_2 on further heating.

To conclude, in the slow-heating mode/annealing the two following phase sequences are observed:

$$\text{As-quenched} \rightarrow \alpha^{iv} \rightarrow \alpha^{ii} \rightarrow (Ni_9S_8 + Ni_3S_2) \rightarrow Ni_{7\pm x}S_6 \qquad [A]$$

$$\text{As-quenched} \rightarrow \alpha^{iv} \rightarrow \alpha^{iii} \rightarrow (Ni_9S_8 + Ni_3S_2) \rightarrow Ni_{7\pm x}S_6 \qquad [B]$$

A related thermal evolution/phase sequence of $Ni_{7\pm x}S_6$ is observed by use of the step-wise heated adiabatic calorimeter. Thus, in the earlier heat capacity study (see series I in Fig. 4 in Ref. 13) three small heat capacity effects occurred for the as-quenched sample with maxima at ~415, 515, and 535 K. Most probably the as-quenched sample converts into α^{iii} during the measurements up to 415 K, where an exothermal transformation takes place. The exothermal effect is noted by a positive noninstrumental temperature-drift rate in the equilibration periods. The phase transformation is not observed in subsequent series of measurements after annealing the sample at 485 K, since the exothermal conversion of α^{iii} is irreversible. It should be noted that the X-ray diffraction pattern of the phase formed exothermally at 415 K could not be distinguished from α^{iii}, a fact which will be discussed further below.

The two higher-temperature effects take place within narrow temperature ranges. The exothermal effect at ~515 K (superimposed on the larger endothermal effect—the maximum of the exothermal reaction would otherwise be observed at higher temperatures) indicates formation of the stable two-phase mixture of Ni_9S_8 and Ni_3S_2, whereas the endothermal effect at ~535 K signals conversion of the exothermally formed phase to α^{i}-Ni_7S_6 (termed α^{i}; see also the next section). The effects disappear after annealing

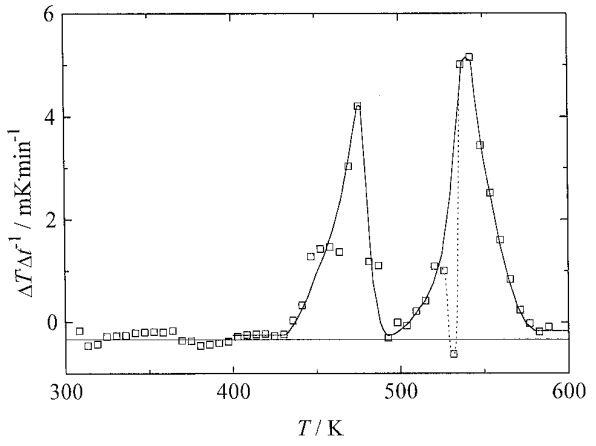

FIG. 3. Individual temperature drift rates in the equilibration periods after each energy input as determined by adiabatic calorimetry.

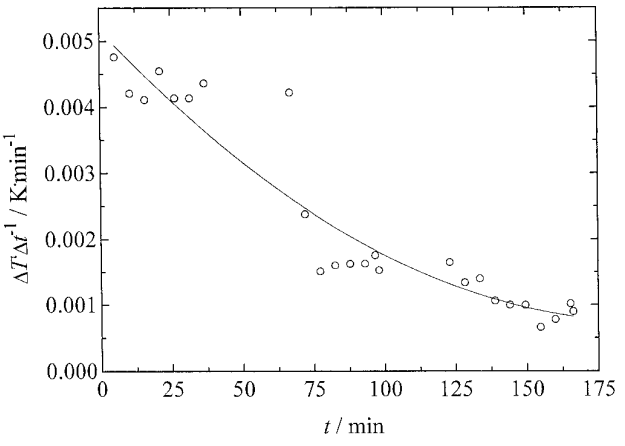

FIG. 5. Temperature drift rate as a function of time after an energy input at 478 K.

at 560 K with resulting formation of the stable products; see ref. (13).

The previously used Ni_7S_6 sample was quenched once more and then annealed at 353 K for 3 months. Thus, pure metastable α^{iii} was obtained as starting material for new heat-capacity measurements. Figure 3 shows the individual temperature drift rates after each energy input as a function of the calorimeter temperature, whereas Fig. 4 shows the resulting heat capacity increments relative to the background heat capacity. A small and steady temperature drift rate prevails up to about 430 K where a slow exothermal process begins (corresponding to the 415 K transformation observed in the previous calorimetric experiment). Since the exothermal effect decayed very slowly (and thus indicated unduly long equilibration periods), the measurements were continued. The temperature drift rate rose to a maximum of approximately 4 mK · min^{-1} at ~475 K, and then decreased abruptly. At somewhat higher temperatures, between 500 and 580 K, a second small exothermal effect referring to formation of the stable two-phase mixture of Ni_9S_8 and Ni_3S_2 was observed. Superimposed on this exothermal signal, a smaller endothermal effect appears at ~530 K; see Fig. 3. The endothermal effect signals the formation of α^{i}. In the present study the exothermal effects are displaced ~50 K higher in temperature compared to those observed earlier for the as-quenched sample (13). The initial extensive annealing of the α^{iii} phase may possibly favor ordering of the Ni atoms and thus decrease the tendency toward disproportionation into stable products.

The kinetics of the exothermal transformation of α^{iii}, starting at 430 K, was studied by observing the enthalpy release as a function of time at 478 K; see Fig. 5. The continuously decreasing enthalpy release indicated a homogeneous reaction mechanism, hence the reaction presumably involves displacement of atoms, rather than nucleation of new phases. The exothermal process most probably relates to a significant change in the structure of α^{iii} since it is observed in two independent calorimetric experiments. In the last experimental series, the sample was thoroughly annealed to produce a single phase α^{iii} sample. For that reason it is not likely that the exothermal reaction signals that trace amounts of α^{iv} or α^{ii} transform to α^{iii}. So far powder X-ray diffraction has not been successful in delineating any structural change connected with this exothermal effect.

Thus, by adiabatic calorimetry, the following phase sequence was observed:

$$\text{As-quenched}/\alpha^{iv} \rightarrow \alpha^{iii} \rightarrow \alpha^{iii}\text{-mod.} \rightarrow \alpha^{i} + (Ni_9S_8 + Ni_3S_2) \rightarrow Ni_{7\pm x}S_6 \quad [C]$$

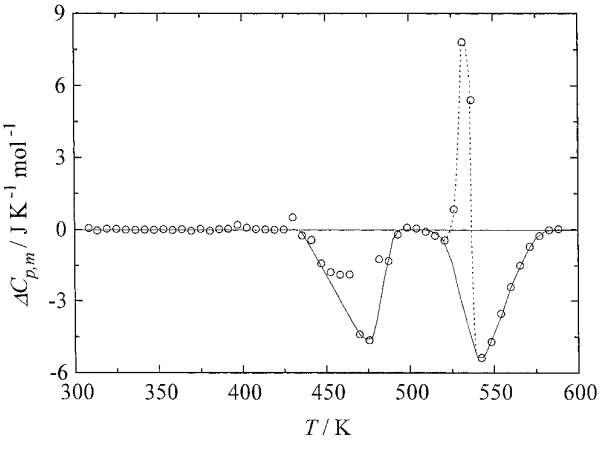

FIG. 4. Deviation of the measured heat capacity from the smoothed nontransitional heat capacity of $Ni_{7\pm x}S_6$ as determined by adiabatic calorimetry.

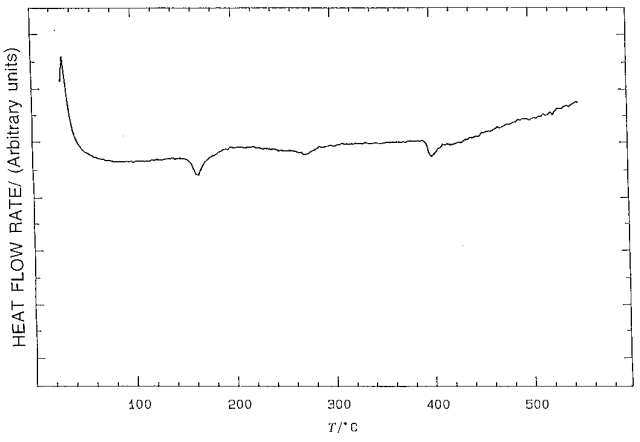

FIG. 6. Heat flow rate on heating α^{iv}.

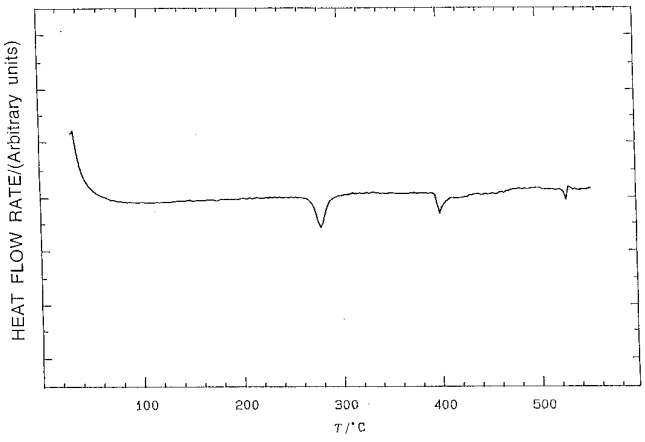

FIG. 7. Heat flow rate on heating α^{iii}.

(*iii*) *Phase Changes of $Ni_{7\pm x}S_6$ on Rapid Heating and Cooling*

The fast-heating situation for the metastable phases is encountered during DSC, PXD, and TEM experiments. Here, an internally consistent phase sequence is observed; it differs from that described above for the slow-heating mode. On heating the as-quenched $Ni_{7\pm x}S_6$ three endothermal effects are observed by DSC at 430, 550, and 670 K; see Fig. 6. These effects signal the transformation sequence (as verified by X-ray diffraction)

$$\alpha^{iv} \rightarrow \alpha^{ii} \rightarrow \alpha^{i} + (Ni_9S_8 + Ni_3S_2) \rightarrow Ni_{7\pm x}S_6, \qquad [D]$$

in good agreement with Sequence [A]. α^{i} is not observed in the annealing experiments as it is quite unstable kinetically and rapidly transforms to $Ni_9S_8 + Ni_3S_2$. The transformation temperatures depend notably on the thermal history of the samples and may vary by some 30 K.

As result of the transformation into α^{ii} at 430 K the rather diffuse reflections of α^{iv} transform back into sharp Bragg reflections. Discontinuous changes in the Bragg reflections occur, during the transformation, probably without any changes in space group symmetry. TEM experiments also provide evidence for a structural change in the relevant temperature range, as indicated by diffuse streaks (12, 14). The TEM data are collected for small crystal volumes, and the observations are not necessarily fully representative for the bulk changes recorded by PXD, DTA, and calorimetry.

The α^{ii} to α^{i} transition at 550 K is accompanied by slight changes in the Bragg positions (PXD) and in the number of reflections present. TEM indicates a transition from monoclinic to orthorhombic symmetry (12, 14). α^{i} is not stable for longer times at temperatures above 550 K and disproportionates to Ni_9S_8 and Ni_3S_2. During continuous heating of the metastable phases within the X-ray apparatus, some 50% of the metastable α^{i} phase remains until the stability region of $Ni_{7\pm x}S_6$ is reached. Thus the thermal effect observed at 670 K most probably represents the combined effect of the α^{i} to $Ni_{7\pm x}S_6$ transition and the eutectoidal formation of $Ni_{7\pm x}S_6$ from Ni_3S_2 and Ni_9S_8. Note that the α^{i} phase is strongly related to the as-quenched state. The X-ray diffraction patterns are nearly identical.

α^{iii} is not formed under these conditions. Its formation requires long annealing times at about 350 K. Heating of a α^{iii} sample results, however, in a somewhat different thermal behavior, since no effects are registered at low temperatures; see Fig. 7. The following transformation sequence (as seen by DTA and X-ray diffraction) is advanced.

$$\alpha^{iii} \rightarrow \alpha^{i} + (Ni_9S_8 + Ni_3S_2) \rightarrow Ni_{7\pm x}S_6. \qquad [E]$$

This sequence is in some contrast to the situation conveyed by adiabatic calorimetry (Sequence [C]), where an exothermal transformation is observed at around 430 K, but confirms the transformation from α^{iii} to α^{i} without the formation of α^{ii}. The exothermal transformation observed by adiabatic calorimetry is too small and slow (corresponding to a 1 K temperature increase in 4 h at maximum) to be detected by thermal analysis.

High-temperature PXD gives additional information on the nature of the transitions and shows that some of the transformations are quasi-reversible. On cooling without achieving thermal equilibrium, PXD shows that depending on the cooling rate, $Ni_{7\pm x}S_6$ undergoes one of the following transformations (on decreasing cooling rate):

$$Ni_{7\pm x}S_6 \rightarrow \alpha^{i}$$
$$Ni_{7\pm x}S_6 \rightarrow \alpha^{i} \rightarrow \alpha^{ii}$$
$$Ni_{7\pm x}S_6 \rightarrow \alpha^{i} \rightarrow \alpha^{ii} \rightarrow \alpha^{iv}$$
$$Ni_{7\pm x}S_6 \rightarrow \alpha^{i} \rightarrow \alpha^{iii}.$$

The kinetics of the transitions are slow, and rapidly cooled samples are considered to consist of a mixture of strained α^{i} and α^{ii}, with an appearance rather similar to that of the as-quenched samples. It is, however, very difficult to obtain single-phase α^{i} as it is rather unstable. Still it appears to us that α^{i} obtained on quenching is kinetically more stable than α^{i} obtained on heating. Quenching from 720 K during cooling of $Ni_{7\pm x}S_6$ thus gives mainly the expected product. The high-temperature phase, $Ni_{7\pm x}S_6$, may most probably be obtained on quenching using larger cooling rates than presently used.

(*iv*) *Structural Characterization of the Metastable Phases*

Based on the rather complex powder X-ray diffraction results and additional information obtained by transmission electron microscopy (TEM) (12, 14) a preliminary schematic description of unit cells of three of the four different metastable phases can be made. PXD data for α^{iv}, α^{iii}, α^{ii}, and α^{i} as well as $Ni_{7\pm x}S_6$ (the last two referring to the situation at 643 and 743 K, as read from Guinier–Simon photographs) are given in Table 1.

$Ni_{7\pm x}S_6$ is orthorhombic (space group *Bmmb*—nonstandard setting) with $a = 327.4 \pm 0.1$ pm, $b = 1615.7 \pm 0.7$ pm, and $c = 1135.9 \pm 0.4$ pm for $Ni_{1.1658}S$ (7). TEM studies on heating show that there is a rather close relation between the lattices for α^{iv}, α^{ii}, α^{i}, and $Ni_{7\pm x}S_6$ (14, 15). The relation between the unit cells of $Ni_{7\pm x}S_6$ and α^{ii} appears to be **a** (α^{ii}) = 2**a** ($Ni_{7\pm x}S_6$), **b** (α^{ii}) = 2**b** ($Ni_{7\pm x}S_6$), and **c** (α^{ii}) = **a** ($Ni_{7\pm x}S_6$ + **c** ($Ni_{7\pm x}S_6$). With a basis in the rather sharp Guinier PXD results for α^{ii} at room temperature, trial-and-error indexing (using the TREOR program (27)) turned out to be successful. The lattice is monoclinic, and the refined unit cell dimensions are $a = 623.8 \pm 0.1$, $b = 3283.0 \pm 0.4$, $c = 1159.6 \pm 0.1$ pm and $\beta = 101.83 \pm 0.01°$. The *b*-axis for α^{i} appears to be half of that for α^{ii}, whereas the monoclinic lattice of α^{iv} is probably the same as that of α^{ii}. No information is at hand for α^{iii}. Details of the TEM study and results from Rietveld refinements of powder X-ray and neutron diffraction data will be published separately (12).

DISCUSSION

During this study four different well-defined metastable phases have been observed and to some extent characterized structurally. Their complex PXD patterns are closely related to each other and to $Ni_{7\pm x}S_6$ but contain significant differences. The metastable phases presumably exhibit homogeneity ranges of approximately the same width as that of $Ni_{7\pm x}S_6$. In addition, an exothermal phase transformation is observed in α^{iii}. No changes in the diffraction patterns could be detected, however, in connection with this transformation.

According to structure analysis by Fleet (7), the high-temperature phase $Ni_{7\pm x}S_6$ is strongly disordered with Ni atoms distributed over at least three tetrahedral or square pyramidal sites. Two of the five different crystallographic sites appear to be almost completely filled, which results in that ~22.5 Ni atoms, on the average, are distributed over 36 possible positions. When this highly disordered phase is undercooled, the decomposition into Ni_9S_8 and Ni_3S_2 appears to be slow enough to allow some ordering of Ni atoms with formation of α^{i} and subsequently for formation of the other metastable variants. The ordering is observed by high-temperature PXD, as is verified on quenching. During quenching of $Ni_{7\pm x}S_6$ from 650 to 850 K, neither sufficient time nor thermal energy is available for a diffusion-controlled ordering of the Ni atoms, and the obtained as-quenched samples probably contain crystallites with large strain due to frozen, unfavorable Ni ordering and/or smaller regions of intergrowth between slightly differently ordered variants. The main part of the enthalpy of these phases relates to chemical bonds for the primary coordination polyhedra for the Ni atoms. The required coordination tetrahedra and square pyramids, as occurring in $Ni_{7\pm x}S_6$, Ni_9S_8, and Ni_3S_2, are most probably available also in the quenched phases, as is indicated by the close relationship between the unit-cell dimensions and the small changes in the intensities of the Bragg reflections between the different metastable phases. However, considerations of geometrical closeness between possible Ni sites show that severe restrictions must exist on simultaneous filling of neighboring sites in an equilibrium state. It is hence easy to rationalize that freezing of Ni atoms will cause some unfavorable Ni–Ni interactions, which again may give rise to local structural distortions, which in turn may be manifested through diffuse Bragg reflections, as seen for α^{iv}, which is formed at room temperature on storage of the as-quenched sample. The atomic diffusion necessary for obtaining a relaxed situation can probably rather easily take place at relatively low temperatures.

The present study clearly shows that a large number of different defect orderings can be produced for $Ni_{7\pm x}S_6$. Fast heating gives disordering, whereas long term annealing gives ordering. An overview of the observed transition sequences is given in a schematic Gibbs energy of formation representation, which indicates the relative stability of the different stable and metastable phases; see Fig. 8. The as-quenched state is included tentatively in the diagram, although a Gibbs energy of formation cannot be assigned to the not uniquely defined ''phase.'' The transformation properties on heating are seen to depend on the nature of the starting material. Storing the as-quenched sample at room temperature, or annealing it at very low temperatures, first produces α^{iv} and then α^{iii}. Very long annealing times are needed to produce the stable two-phase mixture of Ni_9S_8 and Ni_3S_2. On heating, both α^{iv} and α^{iii} transform to α^{i} although the α^{ii} phase is formed

TABLE 1

Observed X-Ray Diffraction Patterns for the Stable and Metastable $Ni_{7\pm x}S_6$ Modifications; *d* Values in pm with Visually Assigned Intensity in Parentheses Are Given

α^{iv}-$Ni_{7\pm x}S_6$ at 293 K	α^{iii}-$Ni_{7\pm x}S_6$ at 293 K	α^{ii}-$Ni_{7\pm x}S_6$ at 293 K	α^{i}-$Ni_{7\pm x}S_6$ at 643 K	$Ni_{7\pm x}S_6$ at 743 K
570.7 (m)	569.2 (vw)	568.3 (vw)	412.6 (vw)	569.7 (w)
495.5 (w)	465.3 (vw)	465.5 (vw)	410.5 (vw)	469.8 (w)
466.0 (vw)	407.3 (m)	407.5 (m)	293.6 (w)	411.5 (w)
421.3 (w)	392.4 (w)	392.6 (w)	281.0 (w)	334.9 (vw)
408.0 (m)	331.3 (vw)	326.3 (w)	275.0 (w)	293.8 (m)
363.8 (m)	326.5 (w)	291.1 (m)	272.7 (m)	286.1 (w)
357.1 (vw)	290.7 (st)	287.0 (m)	247.3 (m)	282.0 (w)
340.4 (m)	287.1 (m)	285.4 (m)	245.2 (m)	273.0 (st)
293.7 (m)	283.4 (w)	283.4 (w)	234.4 (w)	248.6 (vw)
292.5 (w)	282.4 (w)	279.4 (w)	226.0 (w)	247.3 (w)
291.2 (m)	279.6 (w)	277.8 (vw)	212.3 (vw)	245.6 (m)
287.6 (vw)	271.5 (w)	273.6 (vw)	198.0 (m)	237.9 (vw)
283.3 (w)	270.0 (st)	272.2 (m)	193.7 (w)	235.0 (w)
279.8 (w)	245.0 (w)	270.1 (st)	188.1 (st)	226.4 (m)
274.7 (m)	243.2 (m)	267.8 (vw)	185.8 (m)	212.7 (m)
270.4 (st)	237.6 (vw)	246.4 (w)	183.8 (st)	198.2 (m)
255.1 (m)	235.4 (w)	245.0 (w)	182.6 (m)	193.6 (w)
251.3 (w)	232.8 (w)	243.4 (m)	179.3 (w)	188.7 (st)
249.2 (vw)	224.1 (m)	237.8 (w)	177.1 (m)	186.5 (m)
246.4 (st)	210.7 (w)	235.6 (w)	174.3 (vw)	184.2 (m)
244.9 (vw)	204.1 (w)	233.0 (w)	172.8 (vw)	183.0 (m)
243.3 (st)	196.3 (m)	224.3 (w)	170.5 (w)	181.8 (w)
235.9 (w)	187.8 (w)	210.9 (vw)	168.9 (vw)	177.6 (m)
234.2 (vw)	186.5 (st)	204.0 (vw)	164.6 (m)	174.2 (vw)
232.6 (w)	184.7 (m)	196.9 (vw)	163.4 (st)	173.0 (st)
226.8 (w)	182.4 (vw)	187.5 (m)		170.8 (m)
224.3 (m)	181.3 (m)	186.5 (st)		165.1 (m)
212.0 (w)	175.9 (m)	184.6 (m)		163.7 (m)
210.5 (m)	172.6 (vw)	183.2 (m)		154.5 (vw)
197.2 (vw)	171.7 (w)	182.4 (vw)		142.8 (vw)
196.0 (m)	170.6 (w)	181.2 (m)		136.5 (vw)
190.3 (w)	169.1 (m)	175.9 (m)		
188.2 (w)	166.5 (vw)	172.7 (vw)		
186.3 (st)	165.7 (vw)	171.5 (m)		
184.8 (m)	162.0 (m)	170.5 (w)		
182.8 (m)	141.3 (w)	169.1 (m)		
181.2 (st)		167.9 (vw)		
179.2 (w)		166.4 (w)		
177.4 (w)		165.7 (vw)		
176.0 (m)		163.1 (vw)		
172.6 (w)		162.0 (m)		
171.6 (w)		141.3 (vw)		
170.4 (w)				
169.2 (m)				

intermediately in the first case. The transitions at 430 and 550 K on rapid heating of as-quenched samples involve rather small changes in the positions of the Bragg reflections. TEM data show that the unit cells are closely related. The basic atomic arrangements are probably quite similar, and the transitions are believed to reflect different degrees of order–disorder transitions in the Ni sublattice. α^{i} is not kinetically stable and transforms rather rapidly into the stable two-phase mixture of Ni_9S_8 and Ni_3S_2. The relative content of the metastable and stable phases hence depends on the heating rate. On slow heating the exothermal transformation to the stable phases dominates the heat capacity (adiabatic calorimetry). The endothermal reaction (α^{ii} to α^{i}) is also observed but is rather small. On fast heating the endothermal heat flow signal (DSC) due to the α^{ii} to α^{i} transition alone is observed as the commercial thermal

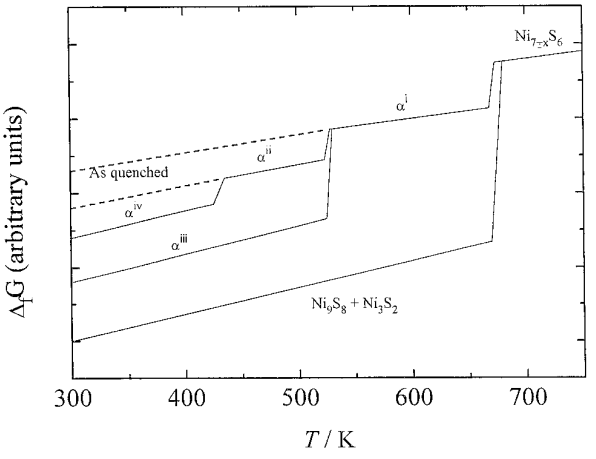

FIG. 8. Schematic Gibbs energy of formation for a sample with composition near $Ni_{7\pm x}S_6$ representation showing the relationship between the different stable and metastable phases.

analysis equipment is much less sensitive. The transitions of $Ni_{7\pm x}S_6$ to α^i, of α^i to α^{ii}, and of α^{ii} to α^{iv} as well as that of α^i to α^{iii} appear to be quasi-reversible. Hence, different phases are obtained, depending on the cooling rate.

It is believed that α^{iv} undergoes an irreversible ordering when forming α^{iii}, whereas a three-step quasi-reversible disordering occurs when transforming via α^{ii} and α^i to $Ni_{7\pm x}S_6$.

The α^{ii} to α^i transition occurs necessarily at a slightly lower temperature than the α^{iii} to α^i transition since the least stable phase has a higher Gibbs energy of formation and should thus intersect the Gibbs energy of formation for the high-temperature phase first. Similarly, the eutectoidal formation of $Ni_{7\pm x}S_6$ probably occurs at slightly higher temperatures than the α^i to $Ni_{7\pm x}S_6$ transition. The temperature differences are, however, not detected by the presently used methods.

The exothermal transformations observed by adiabatic calorimetry for two samples at ~415 and 430 K are not considered in the Gibbs energy representation. The transformations were not detected by powder neutron and X-ray diffraction. Still, it is tempting to suggest that the transformations represent some kind of ordering of the defect structure of the α^{iii} phase. The increased thermal energy at higher temperatures probably makes further ordering of α^{iii} possible and may, hence, explain the effects.

The series of defect ordering observed in the present case is considered to be a more general phenomenon and of more general nature. Similar complex multitudes of metastable phases may presumably be observed in related sulfide systems.

REFERENCES

1. R. Schenk and P. von der Forst. *Z. Anorg. Chem.* **241,** 145 (1939).
2. G. Peyronell and E. Pacilli, *Atti R Accad. Ital. Rend. Cl. Sci. Fis.* **3,** 278 (1942).
3. D. Lundqvist, *Ark. Kemi Mineral. Geol. A* **24,** 12 (1947).
4. T. Rosenqvist, *J. Iron Steel Inst. London* **176,** 37 (1954).
5. M. A. Sokolova, *Dokl. Akad. Nauk SSSR* **106,** 286 (1956).
6. G. Kullerud and R. A. Yund, *J. Petrol.* **3,** 126 (1962).
7. M. E. Fleet, *Acta Crystallogr. Sect. B* **28,** 1237 (1972).
8. M. E. Fleet, *Can. Mineral.* **26,** 283 (1988).
9. E. A. Kulagov, T. L. Evstigneeva, and O. E. Yushko-Zakharova, *Geol. Rudnykh Mestorozhd.* **11,** 115 (1969).
10. A. J. Naldrett, E. Gasparrini, R. Buchan, and J. E. Muir, *Can. Mineral.* **11,** 879 (1972).
11. M. E. Fleet, *Acta Crystallogr. Sect. C* **43,** 2255 (1987).
12. V. Hansen, H. Seim, H. Fjellvåg, and A. Olsen, in preparation.
13. S. Stølen, H. Fjellvåg, F. Grønvold, H. Seim, and E. F. Westrum, Jr., *J. Chem. Thermodyn.* **26,** 987 (1994).
14. V. Hansen, H. Seim, H. Fjellvåg, and A. Olsen, *Micron Microsc. Acta* **23,** 177 (1992).
15. A. Putnis, *Am. Mineral.* **61,** 322 (1976).
16. S. Stølen, F. Grønvold, E. F. Westrum, Jr., and G. R. Kolonin, *J. Chem. Thermodyn.* **23,** 77 (1991).
17. F. Grønvold and S. Stølen, *Thermochim. Acta,* in press.
18. H. Fjellvåg and A. Andersen, *Acta Chem. Scand.* **48,** 290 (1994).
19. R. D. Deslattes and A. Henins, *Phys. Rev. Lett.* **31,** 972 (1973).
20. H. Fjellvåg, and W. Hønle, unpublished data.
21. J. Spreadborough and J. W. Christian, *J. Sci. Instrum.* **36,** 116 (1959).
22. N. O. Ersson, "CELLKANT Program," Chemistry Institute Uppsala Universitet, Uppsala, Sweden, 1981.
23. E. Parthe, K. Yvon, and W. Jeitschko, *J. Appl. Phys.* **10,** 73 (1977).
24. F. Grønvold, *Acta Chem. Scand.* **21,** 1695 (1967).
25. F. Grønvold, *J. Chem. Thermodyn.* **25,** 1133 (1993).
26. S. Stølen and F. Grønvold, *High Temp. High Pressures* **25,** 161 (1993).
27. P. E. Werner, L. Erikson, and M. Westerdahl, *J. Appl. Crystallogr.* **18,** 367 (1985).